



# Optical coherence tomography correlates multiple measures of tissue damage following acute burn injury

Anthony J. Deegan<sup>1</sup>, Samuel P. Mandell<sup>2</sup>, Ruikang K. Wang<sup>1,3</sup>

<sup>1</sup>Department of Bioengineering, <sup>2</sup>Division of Trauma, Critical Care, and Burn, Harborview Medical Center, <sup>3</sup>Department of Ophthalmology, University of Washington, Seattle, WA 98104, USA

*Correspondence to:* Ruikang K. Wang. Department of Bioengineering, University of Washington, 3720 15th Ave. NE, Seattle, Washington 98195, USA. Email: wangrk@uw.edu.

**Background:** The visual assessment of burned skin is inherently subjective, and whilst a number of imaging modalities have identified quantifiable parameters to characterize vascular and structural changes following burn damage, none have become common place in the assessment protocol. Here, we use optical coherence tomography (OCT)-based angiography (OCTA) to introduce novel correlations between vessel depth, i.e., the depth of functional blood vessels beneath the tissue surface, edema depth, i.e., the depth of interstitial fluid buildup beneath the tissue surface, and tissue injury depth, i.e., the depth of collagen denaturation beneath the tissue surface, following burn injury.

**Methods:** A clinical prototype OCT system was used to collect OCT images from various sites of burned skin in patients. Optical microangiography (OMAG) algorithm was used to derive OCTA information from the acquired OCT images, from which the presence of blood vessels and edema were detected. The optical attenuation mapping of structural OCT information was used to detect tissue injury depth. The depths of vessel, edema and tissue injury were measured using a semi-automatic segmentation algorithm. Correlation analysis was performed using a Pearson correlation coefficient using one-tailed analysis with significance being established by a P value  $\leq 0.05$ .

**Results:** Four burn patients were recruited and scanned at multiple sites using the prototype system within 3–6 days of injury. Approximate measurements include a vessel depth range of 320–1,360  $\mu\text{m}$ , an edema depth range of 0–400  $\mu\text{m}$ , and a tissue injury depth range of 130–420  $\mu\text{m}$ . Correlations were subsequently observed between vessel depth and edema depth ( $r=0.8521$ ,  $P=0.0001$ ), and vessel depth and tissue injury depth ( $r=0.6296$ ,  $P=0.0106$ ).

**Conclusions:** OCT is feasible to provide the critical information of vessel depth, edema depth, and tissue injury depth of skin burns, which may represent viable assessment criteria for the characterization of cutaneous burns in future.

**Keywords:** Optical coherence tomography angiography (OCTA); attenuation mapping; skin; burn assessment; vessel depth; edema depth; tissue injury depth

Submitted Feb 19, 2019. Accepted for publication Apr 24, 2019.

doi: 10.21037/qims.2019.04.19

View this article at: <http://dx.doi.org/10.21037/qims.2019.04.19>

## Introduction

Characterizing features of burned skin within a clinical setting is an inherently subjective task that is largely carried out through visual examination by an experienced surgeon (1).

Typically, a surgeon would identify various perfusion or morphological qualities to categorize the burn depth for subsequent treatment planning. Depth categories include superficial (first degree), partial-thickness (second degree),

**Table 1** A comparison between the key features of multiple imaging modalities capable of burn wound assessment. Features compared are: depth of information, resolution, advantages, and disadvantages

Imaging modality	Depth of information	Resolution	Advantages	Disadvantages
Thermography	Tissue surface	100–1,000 $\mu\text{m}$	A potentially high degree of accuracy with a quick data acquisition time and user-friendly features	Only indirect measures of injury depth; Subject to false positive results from ambient heat loss and suffers from decreasing accuracy beyond 3 days post-injury
Ultrasonography	~10 cm	10–1,000 $\mu\text{m}$	Good correlation with histological sections and an improved resolution with high frequency ultrasonography	Requires tissue contact; high resolution is only available with a significant loss of depth of information
Photoacoustic imaging (PAI)	1–5 mm	20–100 $\mu\text{m}$	High resolution with an improved imaging depth	Small field of view and relatively long data acquisition time; has yet to transition beyond pre-clinical
Laser Doppler imaging (LDI)	1–1.5 mm	100–1,000 $\mu\text{m}$	Commercially available and highly correlative with histological assessment	Systems are expensive, bulky and not user-friendly; highly susceptible to tissue variations; no depth information
Laser speckle imaging (LSI)	Tissue surface	~10 $\mu\text{m}$	A relatively simple system setup with a quick data acquisition time and a large field of view	Lacks both depth information and accurate reproducibility in areas of low blood flow
Hyperspectral and multispectral imaging	Tissue surface	~10 $\mu\text{m}$	High resolution with a reduced data acquisition time and cost	Both lack depth information and are very recent additions to the medical imaging field
Optical coherence tomography (OCT)	1–2 mm	1–10 $\mu\text{m}$	Numerous technical variations and functional additions provide both structural and vascular information in 3D with high resolution	Limited imaging depth and field of view; highly sensitive to patient movements

of which there are two further subdivisions: superficial and deep, and full-thickness (third degree), with each having associated features. Superficial burns, for example, would typically show signs of vasodilation and erythema, with intact epidermal and dermal layers (2). Superficial partial-thickness burns would show signs of capillary damage, blistering and edema, as well as epidermal loss and minimal dermal damage (3). Deep partial-thickness burns characteristically show signs of serious vascular damage leading to occlusion, thrombosis and edema, as well as grave epidermal and dermal damage (4). And full-thickness burns demonstrate signs of critical vascular occlusion with complete devastation of the epidermal and dermal layers (4). Despite the invaluable expertise of assessing surgeons, however, the accuracy of such visual examinations has been reported to be just 70–80% (5). This may, in part, be due to the difficult task of identifying features that are located below the tissue surface or those that are visually

indistinguishable next to more profound acute injury responses.

To augment the surgeon's diagnostic abilities, a number of imaging modalities have been investigated for use as possible aides in identifying meaningful features (6). These include ultrasonography and photoacoustic imaging (7), laser Doppler (8) and laser speckle imaging (9), as well as hyperspectral (10) and multispectral imaging (11), and more. Comparative features of a number of key imaging modalities are outlined in *Table 1*. Despite all successfully identifying important features, however, visual examination remains the primary mode of assessment for the characterization and categorization of burned skin. For that reason, we present alternative assessment criteria using optical coherence tomography (OCT)-based angiography (OCTA) and attenuation mapping to identify correlations between vessel depth, edema depth, and tissue injury depth.

OCT is a non-invasive imaging modality that uses near

infrared light in a similar way to how ultrasonography uses sound, to produce cross-sectional images and three dimensional (3D) volumetric scan information (12,13). OCTA is a functional extension of OCT, which adds the capability of visualizing functional microvascular networks beneath the tissue surface (14-17). Such a technique is ideal for identifying subsurface features not ordinarily perceptible through visual assessment. The versatility of OCT has been demonstrated through its use in various forms for burn assessment, such as polarization-sensitive OCT (PS-OCT) (18), spectroscopic OCT (SOCT) (19), and swept-source OCT (SS-OCT) (20), but how OCTA differs from its previous OCT counterparts lies in its ability to image and measure functional blood flow, fluid buildup, and structural features in one single scan. OCTA has previously been used to measure both vascular and structural features in small scale wound models (21-23), and whilst both vascular and structural features have previously been investigated as burn assessment criteria (24), we are unaware of them having ever been measured in this way and correlated for a more comprehensive evaluation. Here, we define 'vessel depth' as the depth of the uppermost functional vessels beneath the tissue surface, 'edema depth' as the depth of interstitial fluid buildup beneath the tissue surface, and 'tissue injury depth' as the depth of thermally-denatured collagen beneath the tissue surface. The tissue surface in this case refers to the surface of remaining tissue following injury and subsequent debridement.

## Methods

### *OCT system configuration and image acquisition*

A clinical prototype OCT system (*Figure 1A*) that was specifically developed at the University of Washington was employed in this study. Briefly, the system utilized a 200 kHz swept laser source with a central wavelength of 1,310 nm (infrared range) and spectral bandwidth of 100 nm to provide an axial resolution of ~8  $\mu\text{m}$  in tissue (~11  $\mu\text{m}$  in air). The sample arm was configured as a handheld probe with a 6.5", 1080p display monitor, sample spacer, and disposable contact unit that could quickly and easily be changed between scans (*Figure 1B,C*). A 5X objective lens delivered the probing light onto the skin with an incident power of 5 mW, whilst a paired X-Y galvo scanner formed raster sampling patterns consisting of fast (x-axis) and slow (y-axis) axes. A ring of light-emitting diodes (LED) positioned between the objective lens and contact unit

(*Figure 1C*) illuminated the imaging site so replicable positioning could be carried out in real time by an onboard charge-coupled device (CCD) camera.

For a comprehensive description of how 3D OCT volumetric scans are acquired, please refer to (25). Briefly, 3D volumetric scans were acquired with a field of view of 9 mm  $\times$  9 mm and a penetration depth of 1.5 mm. Each scan required 800 A-lines to produce a single B-frame, and 800 B-frame locations with 4 repeated B-frames in each, to produce a single volumetric scan referred to as a C-scan (25). Each of the 4 repeated, single-location B-frames were then registered into one and optical microangiography (OMAG) was used to extrapolate OCTA information (26), i.e., blood vessel and edema information. Importantly but simply, OMAG operates by using multiple, single location B-frames, 4 in this case, to contrast the movement of particles from within otherwise static tissue (15,27). In this way, blood vessels are identified by contrasting the movement of red blood cells through functioning blood vessels, and edema is identified by contrasting the movement of now cell- and debris-filled interstitial fluid through the interstitium of burned tissue. In addition to OCTA information mining, each scan also underwent optical attenuation coefficient mapping to obtain tissue injury information (28) from structural information. These methods provided both vascular and structural information, which was then presented and assessed using individual cross-sectional B-frame images, maximum intensity projected *en face* vascular images, and mean intensity projected *en face* attenuation images.

### *Subject volunteers*

Four burn patients were recruited and scanned within 3–6 days of injury. Multiple scan sites, 2–5, were chosen for each based on a specialist surgeon's evaluation. The use of OCT laboratory equipment was approved by the Institutional Review Board (IRB) of the University of Washington. IRB-approved consents were obtained from all subjects before scanning and for the use of unidentified personal and medical information. All procedures adhered to the tenets of Declaration of Helsinki.

### *Data processing*

All depth measurements, i.e., vessel depth, edema depth, and tissue injury depth, were acquired by semi-automatically

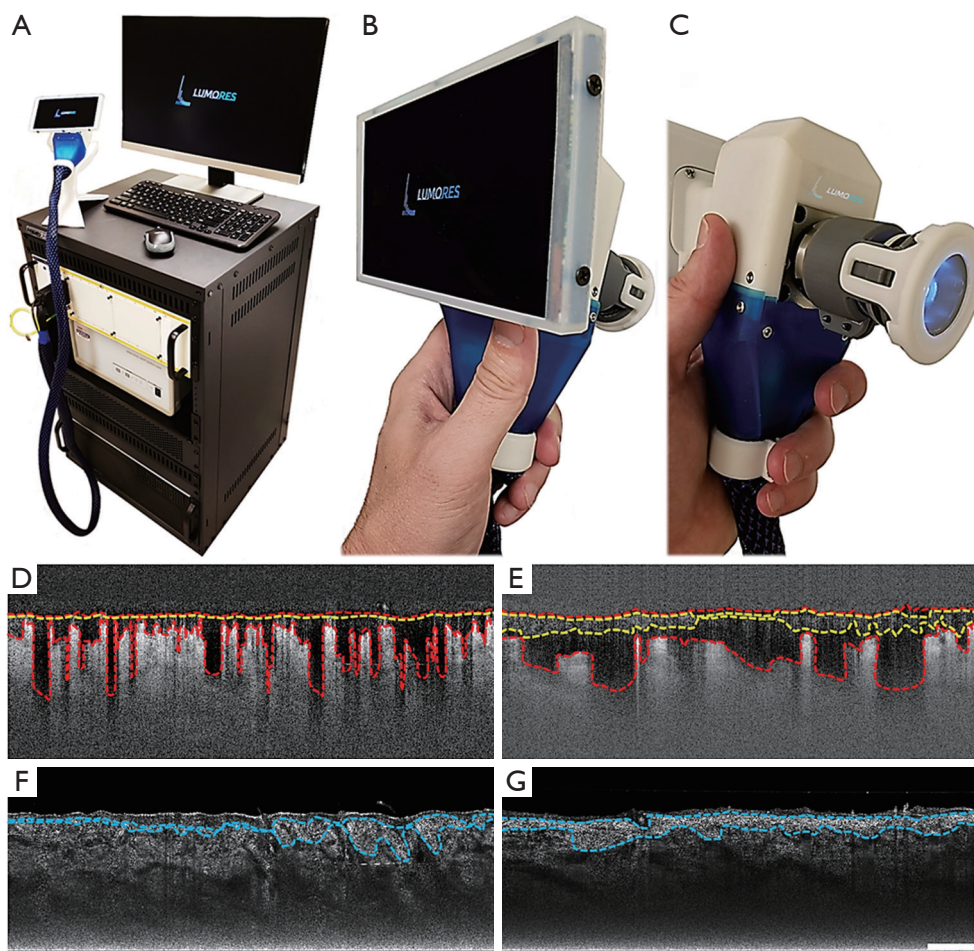


**Figure 1** Images showing the prototype OCT system and handheld probe alongside four cross-sectional B-frame images comparing two different burns. (A) The complete OCT system housed in a self-contained, transportable unit. (B) The handheld probe of the OCT system, highlighting the 6.5", 1080p display monitor and ease of handling. (C) The handheld probe of the OCT system, highlighting the sample spacer, and disposable contact unit. (D) An OMAG-derived cross-sectional B-frame image of an acute skin burn with red perforated lines highlighting tissue surface and vessel depth, and a yellow perforated line highlighting edema. (E) An OMAG-derived cross-sectional B-frame image of a comparable acute skin burn with red perforated lines highlighting tissue surface and vessel depth, and yellow perforated lines highlighting edema boundaries. (F) An attenuation-derived cross-sectional B-frame image corresponding to the burn presented in (D) with blue perforated lines highlighting tissue injury boundaries. (G) An attenuation-derived cross-sectional B-frame image corresponding to the burn presented in (E) with blue perforated lines highlighting tissue injury boundaries. Shown are the boundary lines used for vessel depth, edema depth, and tissue injury depth measurements. Scale bar represents 1 mm. OCT, optical coherence tomography; OMAG, optical microangiography.

outlining boundaries within each of the 800 B-frames that make up each of the 3D volumetric C-scans (29). Vessel and edema information was acquired from OMAG-derived B-frames and tissue injury information from attenuation-derived B-frames. *Figure 1D,E* shows two example OMAG-derived B-frame images highlighting vessel depth (red perforated lines) and edema boundaries (yellow perforated

lines). Both measurements were extracted from each B-frame, compiled, and presented as *en face* vessel depth and edema depth maps with mean  $\pm$  standard error of the mean values. *Figure 1F,G* shows two attenuation-derived B-frame images corresponding to *Figure 1D,E*, respectively, highlighting tissue injury boundaries (blue perforated lines). Again, tissue injury depth measurements were extracted

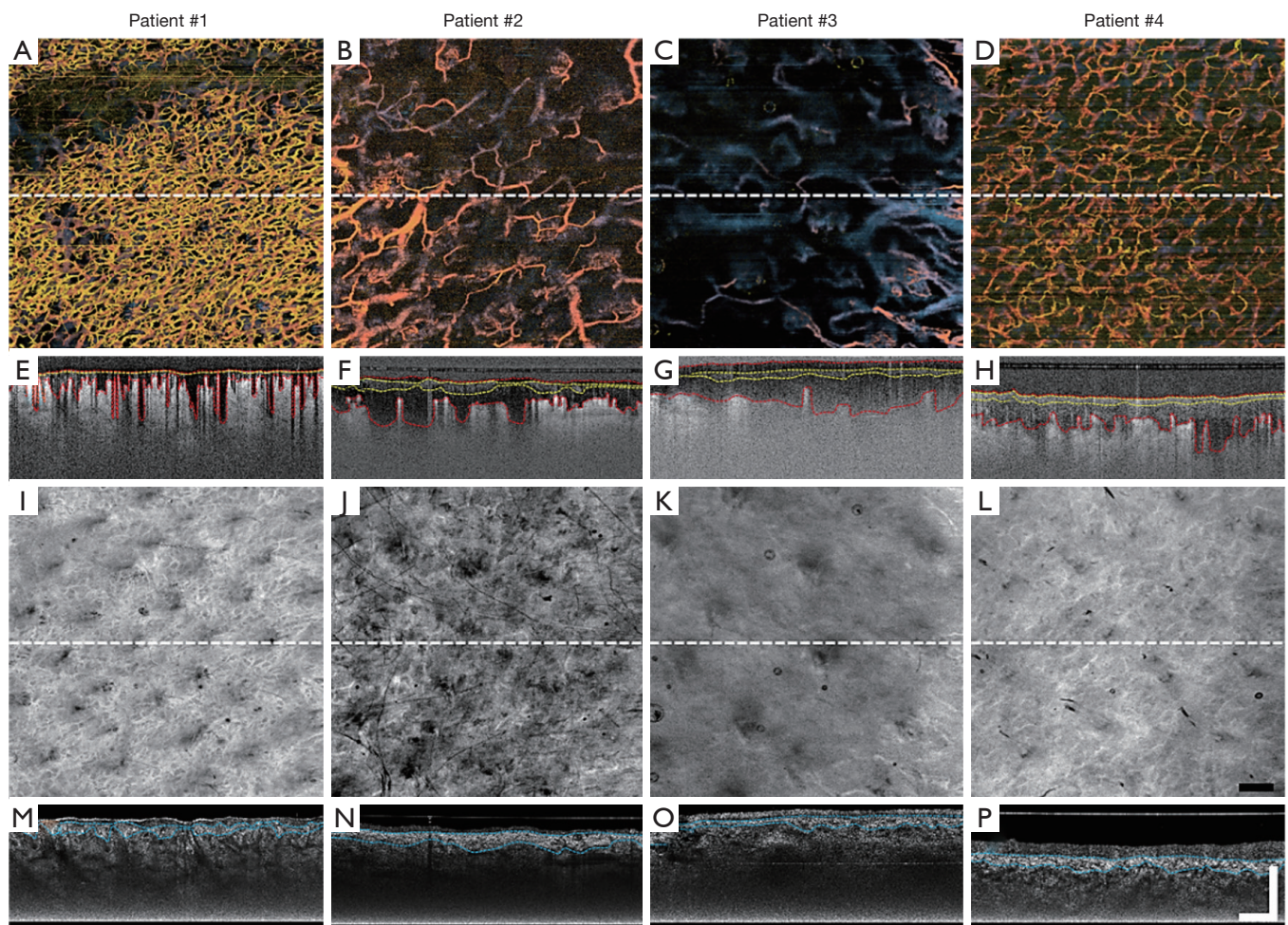


**Figure 2** *En face* and cross-sectional B-frame images derived from OCT scans taken of four burn victims. (A,B,C,D) Maximum intensity projected *en face* vascular images obtained from four burn patients where the vessel depths are color coded from yellow (superficial) to blue (deep) for easier visualization. (E,F,G,H) OMAG-derived cross-sectional B-frame images corresponding to the locations marked by dashed white lines in (A,B,C,D), respectively. Red perforated lines highlight tissue surface and vessel depth, and yellow perforated lines highlight edema boundaries. (I,J,K,L) Mean intensity projected *en face* attenuation images obtained from the tissue surface of four patients depicted in (A,B,C,D), respectively. (M,N,O,P) Attenuation-derived cross-sectional B-frame images corresponding to the locations marked by dashed white lines in (I,J,K,L), respectively. Blue perforated lines highlight tissue injury boundaries. Scale bar represents 1 mm. OCT, optical coherence tomography; OMAG, optical microangiography.

from each B-frame, compiled, and presented as *en face* tissue injury depth maps with mean  $\pm$  standard error of the mean values. Correlation analysis computed a Pearson correlation coefficient using one-tailed analysis with significance being established by a P value  $\leq 0.05$ .

## Results

Visually, the vessels within the burn regions of all four patients differed significantly from one another, as depicted

in their representative *en face* images (Figure 2A,B,C,D). Most notable are differences in vessel density and diameter. This is perhaps most evident when comparing Patient #1 (Figure 2A) with Patient #3 (Figure 2C). This trend continues in the corresponding cross-sectional B-frame images (Figure 2E,F,G,H). In Figure 2E, for example, the presence of small, superficial vessels can still be seen post-injury; however, similar-sized vessels are not evident in Figure 2G. A more obvious feature visible in these B-frame images is vessel depth and how it differs between all

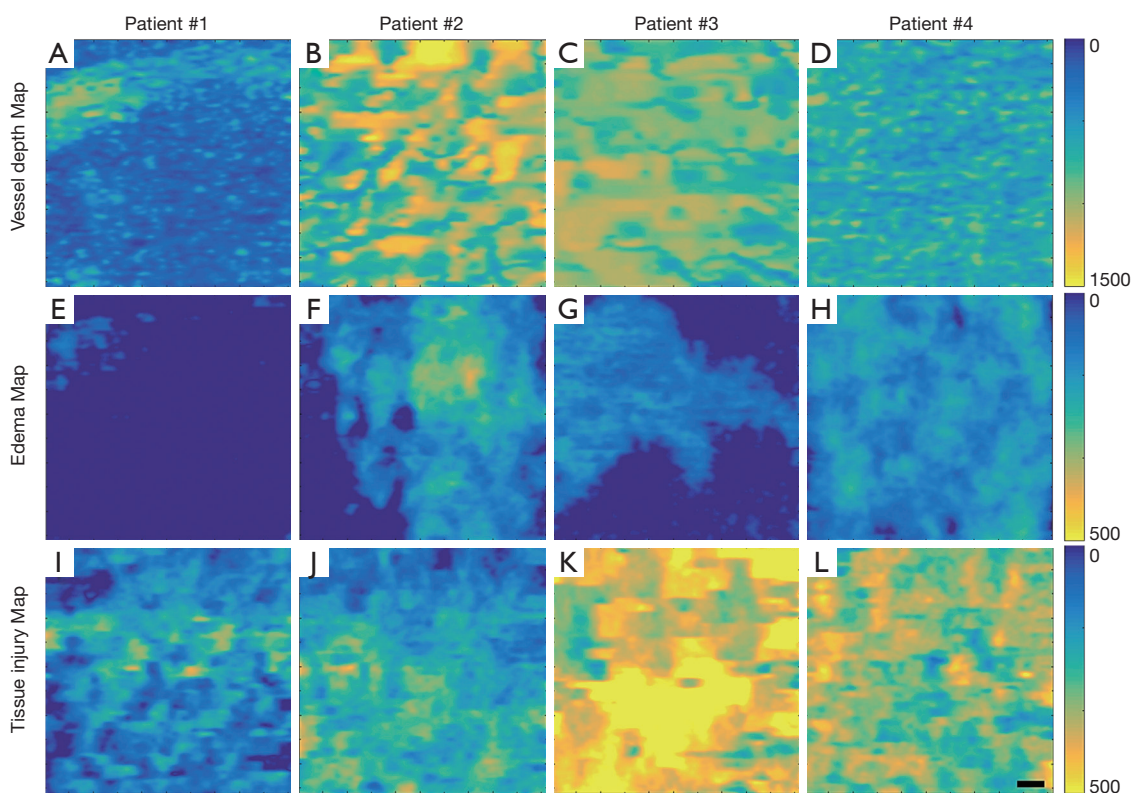


**Figure 3** Vessel depth, edema depth, and tissue injury depth maps. (A,B,C,D) Vessel depth maps derived from the OCTA information of four burn victims. Adjacent color bar represents vessel depth from 0–1,500  $\mu\text{m}$ . (E,F,G,H) Edema depth maps derived from the OCTA information of four burn victims, corresponding with (A,B,C,D), respectively. Adjacent color bar represents edema depth from 0–500  $\mu\text{m}$ . (I,J,K,L) Tissue injury depth maps derived from the attenuation mapping of four burn victims, corresponding with (A,B,C,D) and (E,F,G,H), respectively. Adjacent color bar represents tissue injury depth from 0–500  $\mu\text{m}$ . Scale bar represents 1 mm. OCTA, optical coherence tomography angiography.

four patients, as highlighted by the red perforated lines (Figure 2E,F,G,H). Additionally, in these same example B-frame images, edemas of altering depths beneath the tissue surface become evident, as highlighted by the yellow perforated lines (Figure 2E,F,G,H). Comparing Patient #1 (Figure 2E) with Patient #3 (Figure 2G) again, edema depths vary considerably and appear to correspond with vessel depth. That is, the deeper the blood vessels, the deeper the edema. Structurally, differences can again be seen between patients through attenuation mapping of the tissue surface (Figure 2I,J,K,L). The true extent of these differences, however, remains unclear until subsurface features are assessed via the attenuation-derived cross-sectional B-frame images (Figure 2M,N,O,P). Here, attenuation mapping has highlighted the presence of bright structural features beneath the tissue surface, as highlighted by blue perforated lines (Figure 2M,N,O,P).

Representative vessel depth maps for each patient further highlight patient-dependent variances (Figure 3A,B,C,D), where those patients with deeper vessels have more green-yellow colors present in their maps. Similarly, representative edema depth maps (Figure 3E,F,G,H) and tissue injury depth maps (Figure 3I,J,K,L) too show significant differences between each patient (Figure 3E,F,G,H), where those patients with deeper edema and deeper tissue injury again have more green-yellow colors present in their maps.

Quantitative comparisons between vessel depth, edema depth, and tissue injury depth are shown in Figures 4, 5. Vessel depth measurements are plotted against edema depth measurements from each individual patient in Figure 4A,B,C,D, alongside a comparison between all four patients in Figure 4E. A correlation graph plotting both measures is shown in Figure 4F. Correlation analyses showed a strong correlation with  $r=0.8531$  (95% CI: 0.5675–0.9548,  $P=0.0001$ ).

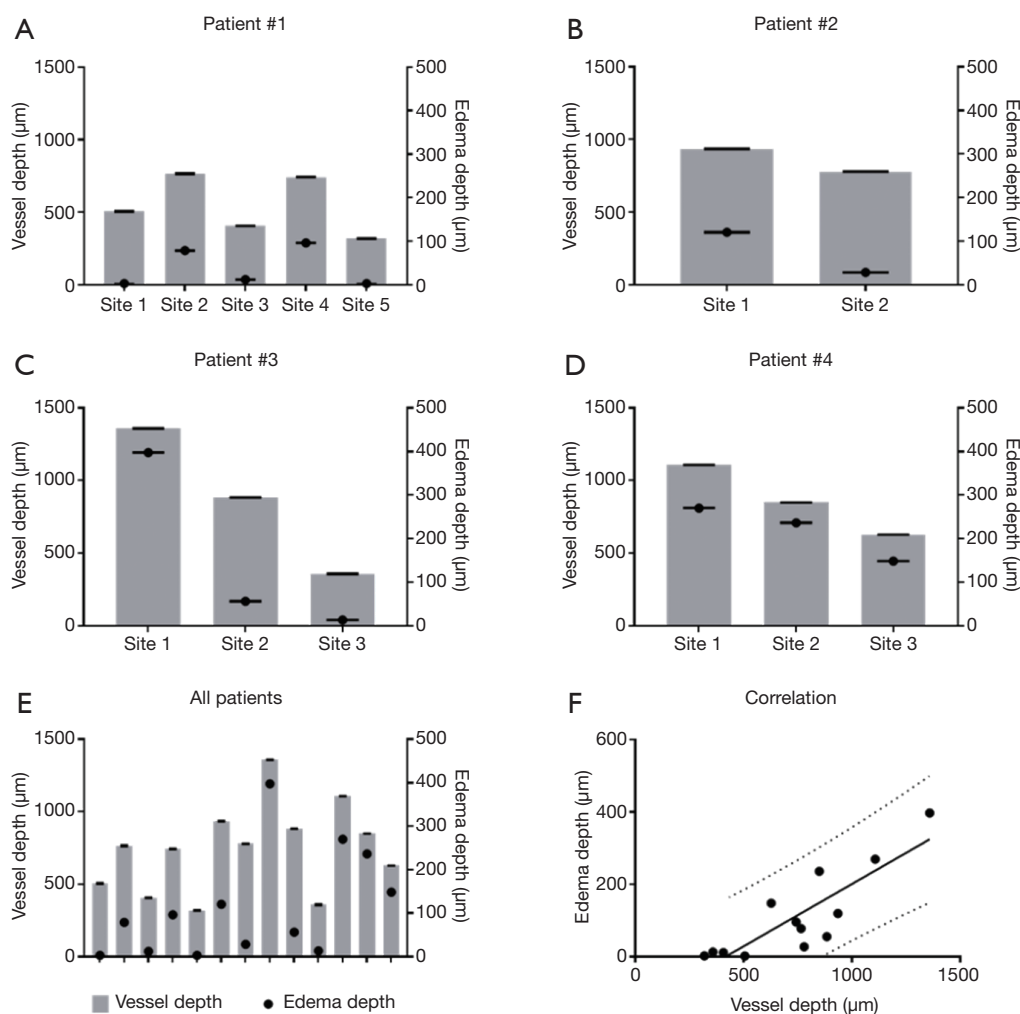


**Figure 4** Graphic representation of vessel and edema depth measurements derived from OCT scans taken of four burn victims. (A) Measurements taken from five scans of Patient #1. (B) Measurements taken from two scans of Patient #2. (C) Measurements taken from three scans of Patient #3. (D) Measurements taken from three scans of Patient #4. (E) Measurements taken from all four patients. (F) Both measures from all four patients plotted as a correlation. Straight black line represents trend. Perforated lines represent 95% prediction bands. Error bars represent standard error of the mean.

Similarly, vessel depth measurements are also plotted against tissue injury depth measurements from each individual patient in *Figure 5A,B,C,D*, alongside a comparison between all four patients in *Figure 5E*. *Figure 5F* shows a correlation graph for both measures. Correlation analyses showed a strong correlation with  $r=0.6296$  (95% CI: 0.1203–0.8765,  $P=0.0106$ ).

## Discussion

Here, we used OCT to show for the first time a good correlation between measures of vessel depth, edema depth,

and tissue injury depth following acute burn damage to the skin. As mentioned, numerous variations of OCT have previously been used to characterize features of burned tissue (18–20) and whilst OCTA has already been used to investigate the characteristics of small scale wound models (21,23), it has never before been used to image large scale, treatment worthy burn wounds. The ability of this technique, however, to capture both vascular and structural information simultaneously makes it a particularly attractive modality for imaging conditions with such multifaceted and intertwined vascular and structural features.

How the skin's vasculature reacts post-burning has long

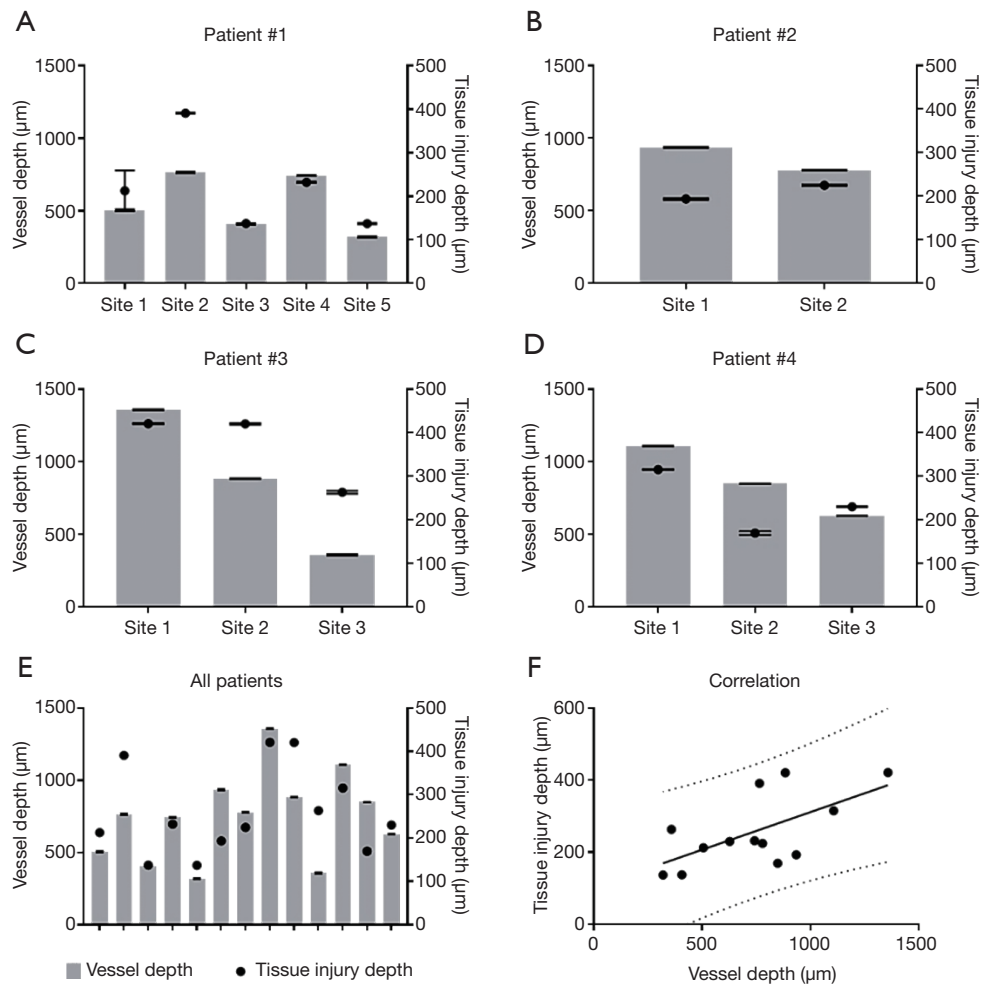


**Figure 5** Graphic representation of vessel and tissue injury depth measurements derived from OCT scans taken of four burn victims. (A) Measurements taken from five scans of Patient #1. (B) Measurements taken from two scans of Patient #2. (C) Measurements taken from three scans of Patient #3. (D) Measurements taken from three scans of Patient #4. (E) Measurements taken from all four patients. (F) Both measures from all four patients plotted as a correlation. Straight black line represents trend. Perforated lines represent 95% prediction bands. Error bars represent standard error of the mean. OCT, optical coherence tomography.

been a topic of interest since local tissue perfusion is known to correlate with the degree of skin damage (2-4); therefore, by measuring how tissue perfusion has changed following an acute burn, one can categorize said burn. Here, we have provided an indirect measure of tissue perfusion through vessel depth and correlated this measure with both edema depth and tissue injury depth. The presence of functional blood vessels was highlighted here using OMAG, which uses the movement of erythrocytes, red blood cells, as an intrinsic contrast agent (26) enabling the detection of actively perfused vessels. Vessel depth, defined as the depth of the uppermost perfused blood vessels beneath the tissue

surface, was subsequently measured using a semi-automatic segmentation algorithm (29). This is thought to signify the degree of vascular occlusion following acute injury to the skin; therefore, indirectly representing the degree of diminished tissue perfusion. An additional parameter to further assess the vascular health of a tissue, burned skin in this case, is the detection of edema. Edema refers to the abnormal accumulation of interstitial fluid and macromolecules within the intercellular space of tissues (30,31); the presence of which is a known characteristic of partial thickness, or second degree, burns (3,4) due to an increase in microvascular permeability and strongly negative

pressure shifts (32) within the burned tissue. Therefore, by detecting the presence of edema and measuring its depth, one could offer an additional measure of vessel damage for burn categorization. Here, the presence of edema was detected using OMAG to distinguish the movement of leukocytes, erythrocytes and other cell types and cellular debris within the interstitial fluid of the edema (exudate) (33). The depth of such was measured and correlated with vessel depth, further compounding the importance of vessel depth measuring for burn assessment. The strong correlation between both measures ( $r=0.8521$ ,  $P=0.0001$ ) is considered a solid indication of the degree of vascular damage and subsequent perfusion arrest. An additional measure of tissue damage, i.e., tissue injury depth, was highlighted from OCT structural information using optical attenuation coefficient mapping; thought here to highlight the presence of denatured collagen because thermal influences are known to transform collagen from a rod-like  $\alpha$ -helix into a random-coil conformation (34,35). Such collagen damage has previously been correlated with alterations in birefringence using OCT (36-38). By measuring the depth of collagen denaturation, i.e., tissue injury, and correlating such with vessel depth ( $r=0.6296$ ,  $P=0.0106$ ), a more comprehensive evaluation of tissue damage is offered. All three measures taken together offer the assessor an opportunity to investigate multiple parameters of subsurface tissue characteristics that would be impossible to measure through visual assessment, or would otherwise require multiple imaging modalities.

It should be noted, however, that there are limitations to this study. Firstly, the cohort recruited here would not suffice for a more comprehensive clinical investigation; secondly, semi-automatically identifying vessel depth, tissue injury depth, and edema depth is both subjective and time consuming; and lastly, a supporting assessment technique may be a useful corroborative tool. Whilst these limitations are not thought to take from the data presented here, they should be addressed in future studies. Developing a fully-automated boundary-identifying algorithm, for example, would aid in the reduction of subjectivity and streamline processing practices for a larger cohort. Using an additional assessment technique, such as histological staining, could also confirm the suspected depth boundaries identified here with OCTA and attenuation mapping. It should also be noted that this study was not intended to categorize the burns shown; rather, it was our intention to use OCTA and attenuation mapping to demonstrate an additional assessment criterion and bring attention to previously

unreported correlations, so they may be considered for use in future larger clinical studies.

## Conclusions

In conclusion, OCT/OCTA has been shown here to be capable of correlating vessel depth with edema depth and tissue injury depth in acute skin burns, which may represent a viable assessment criterion for the categorization of burns in the future.

## Acknowledgments

The study was supported in part by generous supports received from Washington Research Foundation in Seattle, and the American Association for the Surgery of Trauma Research and Education Fund Scholarship.

## Footnote

*Conflicts of Interest:* Dr. Wang discloses intellectual property owned by the Oregon Health and Science University and the University of Washington. The other authors have no conflicts of interest to declare.

*Ethical Statement:* The use of OCT laboratory equipment was approved by the Institutional Review Board (IRB) of the University of Washington and written informed consent was obtained from all patients.

## References

1. Jaskille AD, Shupp JW, Jordan MH, Jeng JC. Critical review of burn depth assessment techniques: Part I. Historical review. *J Burn Care Res* 2009;30:937-47.
2. Kaczmarek M, Nowakowski A, Renkielska A. Rating Burn Wounds by Dynamic Thermography. *Quant Infrared Thermogr J* 2000;5:376-81.
3. Shupp JW, Nasabzadeh TJ, Rosenthal DS, Jordan MH, Fidler P, Jeng JC. A review of the local pathophysiologic bases of burn wound progression. *J Burn Care Res* 2010;31:849-73.
4. Tanaka R, Fukushima S, Sasaki K, Tanaka Y, Murota H, Matsumoto T, Araki T, Yasui T. In vivo visualization of dermal collagen fiber in skin burn by collagen-sensitive second-harmonic-generation microscopy. *J Biomed Opt* 2013;18:61231.
5. Pape SA, Skouras CA, Byrne PO. An audit of the use of

- laser Doppler imaging (LDI) in the assessment of burns of intermediate depth. *Burns* 2001;27:233-9.
6. Deegan AJ, Wang RK. Microvascular imaging of the skin. *Phys Med Biol* 2019;64:07TR01.
  7. Monstrey S, Hoeksema H, Verbelen J, Pirayesh A, Blondeel P. Assessment of burn depth and burn wound healing potential. *Burns* 2008;34:761-9.
  8. Lotter O, Held M, Schiefer J, Werner O, Medved F, Schaller HE, Rahmanian-Schwarz A, Jaminet P, Rothenberger J. Utilization of laser Doppler flowmetry and tissue spectrophotometry for burn depth assessment using a miniature swine model. *Wound Repair Regen* 2015;23:132-6.
  9. Stewart CJ, Frank R, Forrester KR, Tulip J, Lindsay R, Bray RC. A comparison of two laser-based methods for determination of burn scar perfusion: laser Doppler versus laser speckle imaging. *Burns* 2005;31:744-52.
  10. Calin MA, Parasca SV, Savastru R, Manea D. Characterization of burns using hyperspectral imaging technique - a preliminary study. *Burns* 2015;41:118-24.
  11. Thatcher JE, Squiers JJ, Kanick SC, King DR, Lu Y, Wang Y, Mohan R, Sellke EW, DiMaio JM. Imaging Techniques for Clinical Burn Assessment with a Focus on Multispectral Imaging. *Adv Wound Care (New Rochelle)* 2016;5:360-378.
  12. Huang D, Swanson EA, Lin CP, Schuman JS, Stinson WG, Chang W, Hee MR, Flotte T, Gregory K, Puliafito CA, Fujimoto JG. Optical coherence tomography. *Science* 1991;254:1178-81.
  13. Tomlins PH, Wang RK. Theory, developments and applications of optical coherence tomography. *J Phys D Appl Phys* 2005;38:2519.
  14. Wang RK, Jacques SL, Ma Z, Hurst S, Hanson SR, Gruber A. Three dimensional optical angiography. *Opt Express* 2007;15:4083-97.
  15. An L, Qin J, Wang RK. Ultrahigh sensitive optical microangiography for in vivo imaging of microcirculations within human skin tissue beds. *Opt Express* 2010;18:8220-8.
  16. Zhang A, Zhang Q, Chen CL, Wang RK. Methods and algorithms for optical coherence tomography-based angiography: a review and comparison. *J Biomed Opt* 2015;20:100901.
  17. Chen CL, Wang RK. Optical coherence tomography based angiography. *Biomed Opt Express* 2017;8:1056-1082.
  18. Park BH, Saxer C, Srinivas SM, Nelson JS, de Boer JF. In vivo burn depth determination by high-speed fiber-based polarization sensitive optical coherence tomography. *J Biomed Opt* 2001;6:474-9.
  19. Zhao Y, Maher JR, Kim J, Selim MA, Levinson H, Wax A. Evaluation of burn severity in vivo in a mouse model using spectroscopic optical coherence tomography. *Biomed Opt Express* 2015;6:3339-45.
  20. Singla N, Srivastava V, Mehta DS. In vivo classification of human skin burns using machine learning and quantitative features captured by optical coherence tomography. *Laser Phys Lett* 2018;15:025601.
  21. Qin J, Jiang J, An L, Gareau D, Wang RK. In vivo volumetric imaging of microcirculation within human skin under psoriatic conditions using optical microangiography. *Lasers Surg Med* 2011;43:122-9.
  22. Deegan AJ, Wang W, Men S, Li Y, Song S, Xu J, Wang RK. Optical coherence tomography angiography monitors human cutaneous wound healing over time. *Quant Imaging Med Surg* 2018;8:135-150.
  23. Wang W, Deegan AJ, Men S, Wang RK. Optical coherence tomography angiography and cutaneous wound healing. In: *Dynamics and Fluctuations in Biomedical Photonics XV 10493, 104930D*. International Society for Optics and Photonics, 2018.
  24. Burke-Smith A, Collier J, Jones I. A comparison of non-invasive imaging modalities: Infrared thermography, spectrophotometric intracutaneous analysis and laser Doppler imaging for the assessment of adult burns. *Burns* 2015;41:1695-1707.
  25. Deegan AJ, Talebi-Liasi F, Song S, Li Y, Xu J, Men S, Shinohara MM, Flowers ME, Lee SJ, Wang RK. Optical coherence tomography angiography of normal skin and inflammatory dermatologic conditions. *Lasers Surg Med* 2018;50:183-193.
  26. Wang RK, An L, Francis P, Wilson DJ. Depth-resolved imaging of capillary networks in retina and choroid using ultrahigh sensitive optical microangiography. *Opt Lett* 2010;35:1467-9.
  27. Wang RK. Optical Microangiography: A Label Free 3D Imaging Technology to Visualize and Quantify Blood Circulations within Tissue Beds in vivo. *IEEE J Sel Top Quantum Electron* 2010;16:545-554.
  28. Baran U, Li Y, Wang RK. In vivo tissue injury mapping using optical coherence tomography based methods. *Appl Opt* 2015;54:6448-53.
  29. Yin X, Chao JR, Wang RK. User-guided segmentation for volumetric retinal optical coherence tomography images. *J Biomed Opt* 2014;19:086020.
  30. Traves KP, Studdiford JS, Pickle S, Tully AS. Edema: diagnosis and management. *Am Fam Physician*

- 2013;88:102-10.
31. Lund T, Onarheim H, Reed RK. Pathogenesis of edema formation in burn injuries. *World J Surg* 1992;16:2-9.
  32. Wurzer P, Culnan D, Cancio LC, Kramer GC. 8-Pathophysiology of Burn Shock and Burn Edema. In: *Total Burn Care (Fifth Edition)*. Herndon DN. ed. Elsevier, 2018:66-76.e3.
  33. Scallan J, Huxley VH, Korthuis RJ. Pathophysiology of Edema Formation. Morgan & Claypool Life Sciences, 2010.
  34. Thomsen S. Pathologic analysis of photothermal and photomechanical effects of laser-tissue interactions. *Photochem Photobiol* 1991;53:825-35.
  35. Maitland DJ, Walsh JT Jr. Quantitative measurements of linear birefringence during heating of native collagen. *Lasers Surg Med* 1997;20:310-8.
  36. De Boer J, Srinivas S, Malekafzali A, Chen Z, Nelson J. Imaging thermally damaged tissue by Polarization Sensitive Optical Coherence Tomography. *Opt Express* 1998;3:212-8.
  37. Schoenenberger K, Colston BW, Maitland DJ, Da Silva LB, Everett MJ. Mapping of Birefringence and Thermal Damage in Tissue by use of Polarization-Sensitive Optical Coherence Tomography. *Appl Opt* 1998;37:6026-36.
  38. Pierce MC, Sheridan RL, Hyle Park B, Cense B, de Boer JF. Collagen denaturation can be quantified in burned human skin using polarization-sensitive optical coherence tomography. *Burns* 2004;30:511-7.

**Cite this article as:** Deegan AJ, Mandell SP, Wang RK. Optical coherence tomography correlates multiple measures of tissue damage following acute burn injury. *Quant Imaging Med Surg* 2019;9(5):731-741. doi: 10.21037/qims.2019.04.19